

## Article

# Phosphonium Modified Nanocellulose Membranes with High Permeate Flux and Antibacterial Property for Oily Wastewater Separation

Kun Peng <sup>1,2</sup>, Chenglong Wang <sup>1,2</sup>, Chunyu Chang <sup>2,3,4,\*</sup> and Na Peng <sup>1,\*</sup>

<sup>1</sup> Key Laboratory of Coal Conversion and New Carbon Materials of Hubei Province, School of Chemistry and Chemical Engineering, Wuhan University of Science and Technology, Wuhan 430081, China

<sup>2</sup> College of Chemistry and Molecular Sciences, Wuhan University, Wuhan 430072, China

<sup>3</sup> Engineering Research Center of Natural Polymer-Based Medical Materials in Hubei Province, Wuhan University, Wuhan 430072, China

<sup>4</sup> Laboratory of Biomedical Polymers of Ministry of Education, Wuhan University, Wuhan 430072, China

\* Correspondence: changcy@whu.edu.cn (C.C.); pengna@wust.edu.cn (N.P.)

**Abstract:** Nanocellulose membranes could efficiently separate oily wastewater because of their super-hydrophilic and underwater super-oleophobic property and nano-porous structure. However, the practical application and storage of nanocellulose membranes is limited by their low water permeation flux and easy corrosion by bacteria, respectively. Herein, nanocellulose membranes with high permeate flux and antibacterial property were fabricated by grafting tetrakis(hydroxymethyl) phosphonium chloride (THPC) onto the surface of TEMPO-oxidized tunicate cellulose nanofibers (TCNFs) *via* esterification reaction. The introduction of THPC groups with tetrahedral structure on the surface of TCNFs significantly improved the pore size and interlayer space of nanocellulose membranes, resulting in an increase in water permeation flux. These THPC@TCNF membranes were super-hydrophilic and underwater super-oleophobic, which could effectively separate various oil/water nano-emulsions. Moreover, THPC@TCNF membranes possessed excellent durability, mechanical stability and cycling performance. Due to the presence of positively charged phosphonium groups, THPC@TCNF membranes exhibited excellent antibacterial property against *B. subtilis*, a typical Gram-positive bacterium presenting in oily wastewater. This work provides a simple method to endow nanocellulose membrane with high permeate flux and antibacterial property.

**Keywords:** phosphonium; nanocellulose membrane; high permeate flux; antibacterial property; oily wastewater separation



**Citation:** Peng, K.; Wang, C.; Chang, C.; Peng, N. Phosphonium Modified Nanocellulose Membranes with High Permeate Flux and Antibacterial Property for Oily Wastewater Separation. *Coatings* **2022**, *12*, 1598. <https://doi.org/10.3390/coatings12101598>

Academic Editor: Carlo Antonini

Received: 7 September 2022

Accepted: 19 October 2022

Published: 21 October 2022

**Publisher's Note:** MDPI stays neutral with regard to jurisdictional claims in published maps and institutional affiliations.



**Copyright:** © 2022 by the authors. Licensee MDPI, Basel, Switzerland. This article is an open access article distributed under the terms and conditions of the Creative Commons Attribution (CC BY) license (<https://creativecommons.org/licenses/by/4.0/>).

## 1. Introduction

Oily wastewater produced by the petrochemical industry and human activity has attracted worldwide environmental concern; therefore, high-performance materials for oil/water separation are imminently required [1–3]. In comparison to traditional separation technologies such as coagulation, centrifugation, settling and flotation [4–6], membrane separation technology is the preferred technique in the field of oily wastewater purification due to its advantages of high efficiency, simple operation, small footprint and ability to avoid secondary pollution [7–10]. Various membranes, including polymeric membranes [11,12], ceramic membranes [13] and nanomaterial membranes [14], are widely applied in oily wastewater purification. However, the majority of reported membranes still face the problems of non-biodegradability, expensive raw materials and complex fabrication.

Nanocellulose, as the most plentiful natural polymeric nanomaterial on earth, is widely utilized to construct porous nanomaterials due to its high aspect ratio, high elastic modulus, renewability and biodegradability [15–18]. Nanocellulose membranes could be obtained by vacuum-assisted filtration of nanocellulose suspension [19]. Taking the advantages of

many hydroxyl groups on the surface of nanocellulose, nanochannels are formed in the membrane during the fabrication process, through which water molecules can quickly penetrate [20–23]. On the other hand, surface modification of nanocellulose has been widely reported, which promoted the development of nanocellulose-based membranes in the field of water purification, which could remove dyes, organic compounds, heavy metals and oils from wastewater [24–30]. Nanocellulose membranes could effectively separate oil/water nano-emulsions, which was attributed to the nanoscale pore size and super wettability of the membrane [31]. However, the nano-porous structure of membranes produced by dense assembly of nanocellulose always reduced their permeate flux, which severely limited their separation efficiency [32]. According to the Hagen–Poiseuille Equation (1):

$$J = \frac{\varepsilon r^2 \Delta p}{8\mu L} \quad (1)$$

where  $J$  is the liquid flux through the membrane,  $\varepsilon$  is the surface porosity,  $r$  is the pore size,  $\Delta p$  is the pressure,  $\mu$  is the liquid viscosity and  $L$  is the thickness of the membrane [33]. To improve the permeate flux of membranes, enhancing the pore size (or porosity) and lessening the thickness of membrane are two general strategies [34,35]. By mixing silica particles with bacterial cellulose, the porosity of membrane was significantly increased [36]. The pore size of the membranes could also be enhanced by combining solvent exchange of nanocellulose suspensions with ethanol and the use of a removable template (a mixture of calcium compounds) [37]. On the other hand, ultrathin cellulose Voronoi-nanonet membrane could be fabricated by welding to the electrospinning nanofiber substrate *via* nonsolvent-induced phase separation [38]. Although the permeate flux of these cellulose-based membranes could be effectively improved, they could not efficaciously prevent the corrosion of cellulose by microorganisms and the blockage of the membrane, affecting its service life.

Herein, we tried to fabricate antibacterial nanocellulose membranes with high permeate flux by grafting tetrakis(hydroxymethyl) phosphonium chloride (THPC) onto TEMPO-oxidized tunicate cellulose nanofibers (TCNFs). THPC with flame retardancy and antibacterial property is an inexpensive by-product of phosphine tail gas [39]. Owing to its tetrahedral structure and broad-spectrum antibacterial characteristics [40,41], THPC was employed as pore-forming and antibacterial agent to endow membranes with enlarged pore size and antibacterial property. With successful grafting of THPC, the average pore size and thickness of THPC@TCNF membranes were improved, exhibiting high pure water fluxes. Moreover, the THPC@TCNF membrane can effectively separate oil/water nano-emulsions due to its super-hydrophilic and underwater super-oleophobic properties. In addition, the membranes exhibited good mechanical stability, cycling properties and antibacterial properties.

## 2. Experimental Section

### 2.1. Materials

Tunicate (*Halocynthia roretzi* Drasche) was obtained from Weihai Evergreen Marine Science and Technology Co., Ltd. (Weihai, China). Microporous filter membrane (Nylon 66, cut-off: 0.22  $\mu\text{m}$ , diameter: 50 mm) as a support was bought from Tianjin Jinteng Co., Ltd (Tianjin, China). 2,2,6,6-tetramethyl-1-piperidinyloxy (TEMPO) was purchased from Sigma-Aldrich (America). Tetrakis(hydroxymethyl) phosphonium chloride (THPC, 80% aqueous solution) and 4-dimethylaminopyridine (DMAP, 99%) were purchased from Aladdin Reagent Co., Ltd (Shanghai, China). Sodium hypochlorite (NaClO) was obtained from Alfa Aesar Co., Ltd (Shanghai, China). Sodium bromide (NaBr), sodium hydroxide (NaOH), hydrogen peroxide ( $\text{H}_2\text{O}_2$ ) and dimethyl sulfoxide (DMSO) were obtained from Sinopharm Chemical Reagent Co., Ltd. (Beijing, China). Unless otherwise specified, other reagents were of analytical grade.

## 2.2. Fabrication of Tunicate Cellulose Nanofibers (TCNFs)

Tunicate cellulose was isolated from the mantle of tunicate by NaOH boiling and H<sub>2</sub>O<sub>2</sub> bleaching according to our previous method [42,43]. Afterwards, tunicate cellulose (1 g) was dispersed in deionized water (99 g), followed by the addition of NaBr (0.1 g) and TEMPO (0.016 g). After TEMPO was completely dissolved, NaClO (6.2 g, 12%) was used to start the TEMPO oxidation and NaOH (1 M) was applied to maintain the reaction medium pH of 10~10.5 under 400 rpm stirring for 12 h. Finally, the TEMPO-oxidized tunicate cellulose suspension was centrifuged and dialyzed to neutrality and the TCNF suspension was obtained by mechanical stirring in an ordinary soymilk machine.

## 2.3. Fabrication of THPC@TCNF Membranes

TCNF suspension (12 mL, 0.06 wt.%) was freely deposited on the Nylon 66 supported membrane by vacuum-assisted filtration to obtain a TCNF layer (5.73 g m<sup>-2</sup>). Subsequently, the Nylon 66 membrane coated with TCNF layer was dried and finally stripped from the Nylon 66 support to obtain a self-supporting TCNF membrane. Subsequently, a certain amount of THPC (2~32 wt.%) with DMAP (5 wt.%) was dissolved in DMSO. The TCNF membranes were then soaked with the above solution at room temperature for 24 h. Finally, THPC@TCNF membranes were fabricated by washing with deionized water and drying.

## 2.4. Characterization

The morphologies of TCNFs and THPC@TCNFs were visualized with transmission electron microscopy (TEM, JEM-2100, Tokyo, Japan). A drop of nanofibers suspension (0.05 wt.%) was dropped and evaporated on a copper grid before measurement. The surface and cross-section morphologies of membranes were observed with a scanning electron microscope (SEM, Zeiss, Oberkochen, Germany) operated at 5 kV. The surface and cross-section of samples were sputtered with gold and then observed and photographed. The chemical structures of THPC@TCNF membranes were analyzed with Fourier transform infrared spectrometer (FT-IR, NICOLET 5700, Thermo Fisher Scientific, Waltham, MA, USA). The constituent elements of the membranes before and after modification were analyzed by X-ray photoelectron spectrometer (XPS, ESCALAB250Xi, Thermo Fisher Scientific, Waltham, MA, USA). The distribution of P and Cl element was observed with energy disperse spectroscopy (EDS, Oxford UltimMax 40, Oxford, UK). The wettability of membranes was characterized by contact angle measurements (DSA100, Krüss, Hamburg, Germany). The water contact angle (WCA) data were obtained by placing a drop of deionized water (2.0 µL) on the surface of membranes at room temperature in air. Four different oils, petroleum ether, chloroform, pump oil and dimethicone, were applied to characterize the underwater superoleophobicity of membranes. Oil drops (1.5 µL) were dropped on the surface of the membrane to obtain underwater oil contact angle (OCA) data at room temperature in deionized water.

## 2.5. Oil/Water Nano-Emulsion Separation

Four types of emulsions containing oil droplets of 50~500 nm were prepared by dispersing each of the above four oils into water with the help of surfactants, respectively. Details on the preparation of various nano-emulsions are provided in the Supporting Information. In a typical oil/water nano-emulsion separation process, the effective filter membrane area was 1.54 cm<sup>2</sup> and various nano-emulsions were fed into the separation unit at a constant pressure of 0.5 bar. According to the volume of filtrate collected in 5 min, the water flux  $J$  (L m<sup>-2</sup> h<sup>-1</sup> bar<sup>-1</sup>) was calculated by substituting into Equation (2):

$$J = \frac{V}{At\Delta P} \quad (2)$$

where  $V$  (L),  $A$  (m<sup>2</sup>),  $t$  (h) and  $\Delta P$  (bar) are water permeate volume, effective filtration membrane area, permeation time and transmembrane pressure, respectively.

The oil concentration of the filtrates was measured with an infrared spectrometer oil content analyzer (FYHW-2000B, Fangyuan, Wuhan, China). The oil rejection  $R$  (%) was obtained according to Equation (3):

$$R = \frac{C_0 - C_f}{C_0} \times 100\% \quad (3)$$

where  $C_f$  (mg mL<sup>-1</sup>) and  $C_0$  (mg mL<sup>-1</sup>) are the oil concentrations in the filtrate collected after filtration and in the unfiltered oil/water emulsion, respectively. The infrared spectrometer oil content analyzer was used to measure the value of  $C_f$ .

For the cycle performance of THPC@TCNF membranes in the oil/water separation process, the membranes were soaked in pure water for a few seconds after each cycle and dried for the next cycle.

### 2.6. Antibacterial Property

The antibacterial properties of various membranes were appraised using *Bacillus subtilis* (*B. subtilis*), which is a typical Gram-positive bacterium presenting in oily wastewater. In the blend culture test, a complete membrane was soaked in the diluted *B. subtilis* solution (10<sup>7</sup> CFU mL<sup>-1</sup>, 2 mL). After culturing at 37 °C for 1 h, bacterial solution (100 µL) was spread on the Luria-Bertani (LB) culture medium. After culturing at 37 °C for 24 h, the number of colonies was counted. For the bacterial filtration test, the diluted bacterial liquid (10<sup>2</sup> CFU mL<sup>-1</sup>, 10 mL) was deposited on the membranes by vacuum-assisted filtration. The membranes were kept under wet condition for 1 h and then the morphology of bacterial was observed by SEM.

## 3. Results and Discussion

### 3.1. Fabrication and Morphology of THPC@TCNF Membranes

The fabrication process of THPC@TCNF membrane is displayed in Figure 1. Firstly, the TEMPO oxidized TCNF suspension was deposited on a nylon 66 supported membrane by vacuum assisted filtration. After drying, the supported membrane was removed to obtain a self-supporting TCNF membrane (Figure S1a). After TEMPO oxidation, many carboxyl groups appeared on the surface of the TCNFs. By immersing TCNF membrane into THPC solution, THPC was grafted onto the surface of TCNFs in the membrane via esterification reaction. Finally, the THPC@TCNF membrane was obtained after washing with water and drying (Figure S1b). Benefiting from the swelling effect of DMSO, the tetrahedral structure of THPC and the electrostatic repulsion of positively charged phosphonium groups, the pore size and thickness of THPC@TCNF membrane was significantly improved in comparison with TCNF membrane. Therefore, THPC@TCNF membrane was expected to have enhanced permeate flux and antibacterial property.

TCNFs prepared by TEMPO-oxidized tunicate cellulose had fiber-like morphology, whose average length, average width and aspect ratio were 10.0 ± 0.3 µm, 6.5 ± 0.2 nm and ~1540, respectively (Figure S2). The ultralong morphology of TCNFs could be attributed to the high molecular weight and crystallinity of tunicate cellulose [44]. Due to the presence of -COO<sup>-</sup> /-COO<sup>-</sup> electrostatic repulsion [45], TCNFs dispersed well in water and formed stable and homogeneous suspensions (Figure S3).

After vacuum-assisted filtration, TCNF membrane exhibited a nano-porous structure with an average pore size of 50.4 ± 2.5 nm (Figure 2a), which could generate capillary force and easily form a hydration layer during the oil/water separation process [9]. After modification, THPC@TCNF membrane displayed a relatively loose surface with a larger pore size (62.2 ± 2.9 nm), as shown in Figure 2b. According to the Hagen–Poiseuille equation, the enlarged pore size of membranes would improve their permeate flux during oily wastewater purification. Besides, the thickness of TCNF membrane also augmented from 11.8 µm to 21.1 µm after reacting with THPC, while larger pore size could be clearly discovered in the cross-section of THPC@TCNF membrane (Figure 2c). THPC modified TCNFs that, isolated from membrane, had a fiber-like morphology and some black dots

could be observed on the surface of TCNFs (Figure S4). These results indicated that THPC was successfully grafted onto TCNFs via esterification reaction and the morphology of TCNFs was not changed.

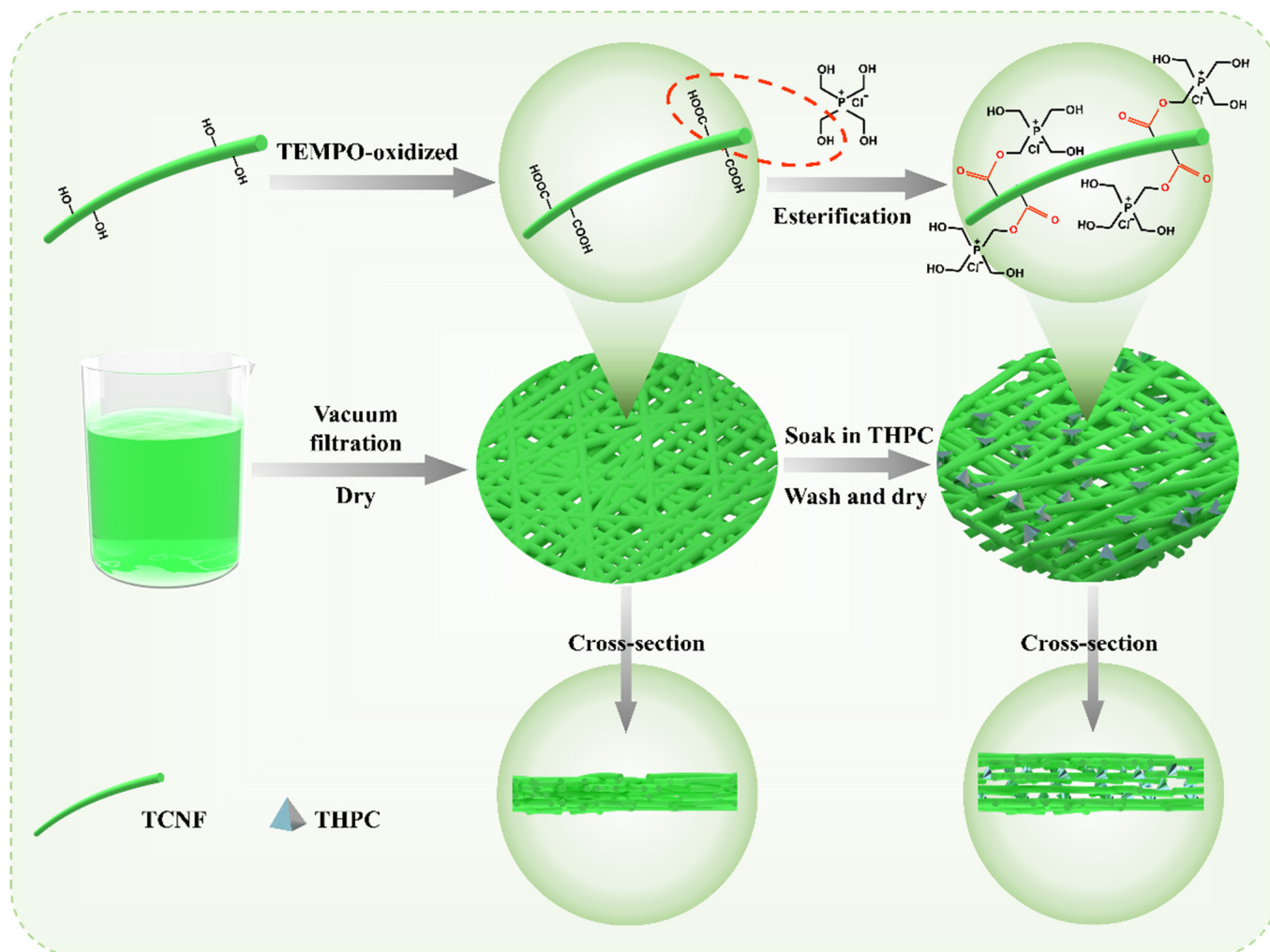


**Figure 1.** Schematic illustration for the fabrication process of THPC@TCNF membrane.

### 3.2. Structure of THPC@TCNF Membranes

To comprehend the chemical structure of THPC@TCNF membrane, FT-IR spectra of TCNF membrane and THPC@TCNF membrane were compared. As displayed in Figure 3a, a new absorption band appeared at  $1725\text{ cm}^{-1}$  in the spectrum of THPC@TCNF membrane, which was ascribed to  $\nu_{\text{C=O}}$  in the ester bond formed through esterification of  $\text{-COOH}$  and  $\text{-OH}$  [46]. The absorption band located at  $3426\text{ cm}^{-1}$  corresponding to  $\text{-OH}$  stretching vibration became stronger in the spectrum of THPC@TCNF membrane due to the introduction of THPC. Moreover, a new characteristic peak at  $133.5\text{ eV}$  could be discovered in the XPS spectrum of THPC@TCNF membrane (Figure 3b), which could be assigned to the phosphorus element of THPC. In the high-resolution  $\text{P}_{2\text{p}}$  spectra, the characteristic peak could only be found in the spectrum of THPC@TCNF membrane (Figure S5), revealing the presence of phosphonium groups. In the  $\text{C}_{1\text{s}}$  spectrum of THPC (Figure 3c), different types of carbon atoms included aliphatic carbon ( $\text{C-H}$ ,  $284.68\text{ eV}$ ), hydroxyls ( $\text{C-O}$ ,  $286.30\text{ eV}$ ) and carbon-phosphorus covalent bond ( $\text{C-P}$ ,  $286.80\text{ eV}$ ), where related peaks shifted to  $284.91$ ,  $286.55$  and  $288.15\text{ eV}$ , respectively, in the spectrum of THPC@TCNF membrane (Figure 3d), indicating that the binding of THPC and TCNFs resulted in a higher binding energy of various types of carbon atoms. Furthermore, a new XPS peak was seen at  $288.15\text{ eV}$  in  $\text{C}_{1\text{s}}$

spectrum of THPC@TCNF membrane, which was assigned to carboxyl groups (O=C=O) due to the presence of TCNFs.

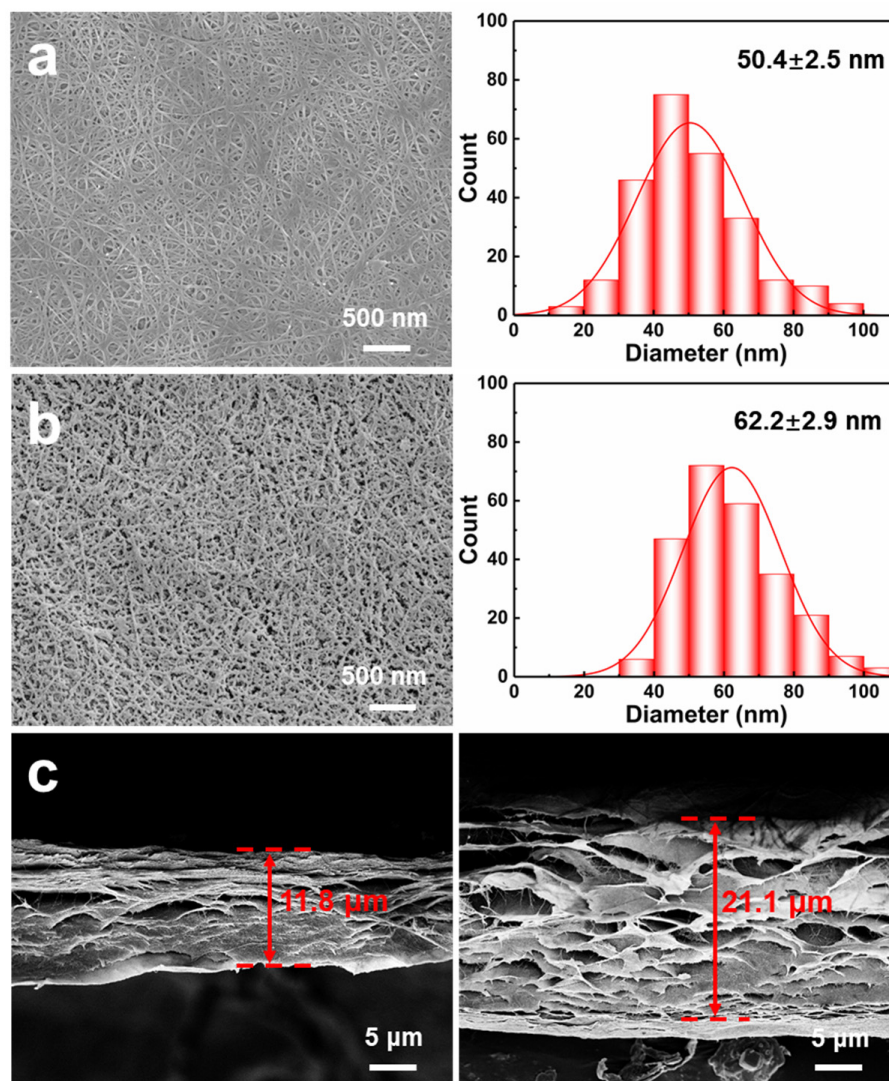


**Figure 2.** SEM images of surface (left) and pore size distribution (right) of (a) TCNF membrane and (b) THPC@TCNF membrane. (c) SEM images of cross-section of TCNF membrane (left) and THPC@TCNF membrane (right).

In addition, the distribution of phosphonium groups in the membrane was also investigated by EDS mapping of P and Cl elements. As shown in Figures 3e and S6, green and red dots were uniformly distributed in the images, revealing that phosphonium groups were uniformly distributed in the membrane. To determine the degree of substitution of phosphonium groups, the carboxyl content of THPC@TCNF membranes prepared with different dosages of THPC was measured by conductance titration. As displayed in the Figure 3f, the carboxyl group content of TCNF membrane was  $1.25 \text{ mmol g}^{-1}$ , because TCNFs were prepared by TEMPO-oxidization strategy and carboxyl groups generated on the surface of TCNFs. When the dosage of THPC increased from 0% to 16%, carboxyl content gradually decreased from 1.25 to  $0.28 \text{ mmol g}^{-1}$ . As the dosage of THPC further increased to 32%, the carboxyl content changed slightly because of the steric hindrance effect of phosphonium groups.

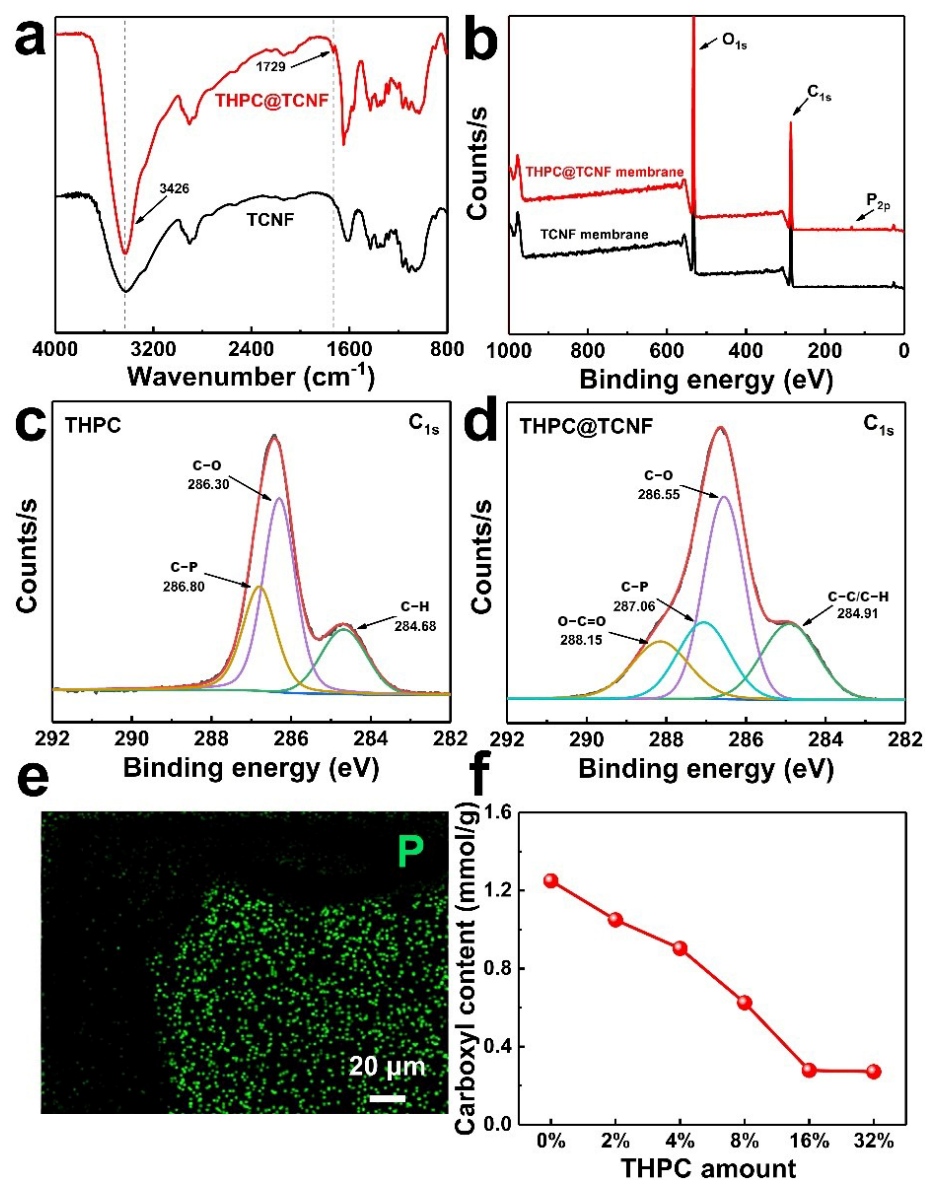


**Figure 3.** (a) FT-IR spectra and (b) XPS spectra of TCNF membrane and THPC@TCNF membrane. High-resolution C<sub>1s</sub> spectra of (c) THPC and (d) THPC@TCNF membrane. (e) EDS mapping of phosphorus element on THPC@TCNF membrane. (f) Relationship between carboxyl content of THPC@TCNF and THPC dosage.

### 3.3. Wettability and Separation Performance of THPC@TCNF Membranes

The wettability of the membranes is strongly dependent on their chemical composition and surface topography, which is crucial to the separation efficiency and fouling resistance during oily wastewater purification [47,48]. As shown in Figure 4a, a water droplet could quickly spread out on the surface of THPC@TCNF membrane in air, indicating the superhydrophilicity of membrane. Four kinds of oils, including petroleum ether, pump oil, dimethicone and chloroform, were employed to study the wettability of THPC@TCNF membrane. The underwater oil contact angles were 158.7°, 164.6°, 160.4° and 158.1° for petroleum ether, pump oil, dimethicone and chloroform, respectively (Figure 4b). These results indicated that various oil droplets with different density and viscosity could be repelled by the THPC@TCNF membranes, revealing their underwater super-oleophobic properties. The wettability of THPC@TCNF membranes was consistent with that of TCNF membranes (Figure S7), which confirmed that the introduction of THPC into TCNF membranes did not change their wettability.

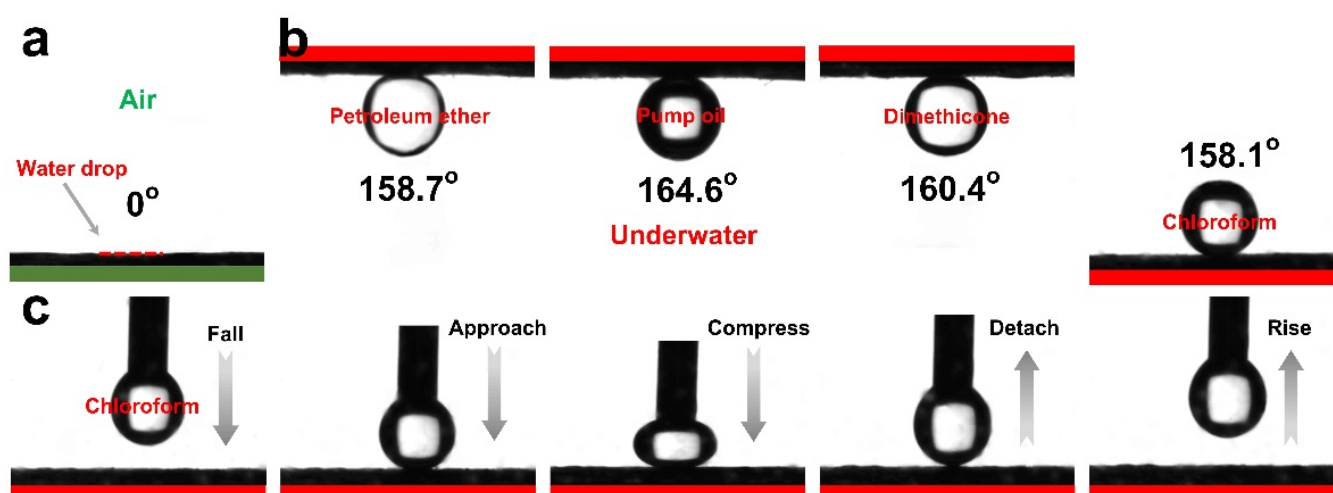


**Figure 4.** Contact angle measurement of THPC@TCNF membranes with respect to wettability. Photograph of a water drop in air (a), underwater various types of oil drops on THPC@TCNF membranes (b). Dynamic approach-compress-detach oil-adhesion test photograph for THPC@TCNF membrane (c).

As exhibited in Figure 4c, the underwater anti-oil adhesion property of the THPC@TCNF membrane was evaluated with a dynamic approach-compress-detach test. Under water, after contacting the surface of the THPC@TCNF membrane, the chloroform droplets were slowly compressed downward to form an ellipse. When gradually lifted, the chloroform droplets could quickly overcome the adhesion force and detach from the THPC@TCNF membrane surface without any deformation. The results illustrated that the THPC@TCNF membrane was expected to have low oil adhesion and excellent antifouling performance during oil/water separation.

To ascertain the optimal dosage of THPC, the water permeate flux of different THPC@TCNF membranes was shown in Figure S8. As THPC dosage increased from 0 to 16 wt.%, the water flux of membranes increased from  $1208 \pm 35$  to  $1931 \pm 64$   $\text{L m}^{-2} \text{h}^{-1} \text{bar}^{-1}$ , which was attributed to the enlarged pore size of the membranes. When the dosage of THPC increased to 32 wt.%, the water permeate flux of membrane was  $1928 \pm 63$   $\text{L m}^{-2} \text{h}^{-1} \text{bar}^{-1}$ . This result agreed with the result for carboxyl content, suggesting that the water permeate flux of membrane was dependence of carboxyl content in the membrane. Thus, THPC@TCNF membrane that was prepared by using 16% THPC was selected for the purification of oily wastewater. Four kinds of oil/water nano-emulsions with average particle size of 200 nm were prepared, which showed a bright pathway under the irradiation of a laser pen because of the Tyndall effect (Figure 5a–d).

After separation, the size of particles in filtrate was reduced to about 2 nm (surfactants), indicating that the oil droplets in the emulsions could be effectively separated by THPC@TCNF membranes. Moreover, the water permeation fluxes and oil rejections of TCNF membrane and THPC@TCNF membrane for the separation of the four nano-emulsions were compared. The water fluxes of TCNF membranes for petroleum ether, chloroform, pump oil and dimethicone nano-emulsions were  $1115 \pm 35$ ,  $989 \pm 28$ ,  $1056 \pm 34$  and  $1094 \pm 35$   $\text{L m}^{-2} \text{h}^{-1} \text{bar}^{-1}$ , respectively, whereas those of THPC@TCNF membranes for petroleum ether, chloroform, pump oil and dimethicone nano-emulsions were  $1858 \pm 58$ ,  $1453 \pm 48$ ,  $1625 \pm 45$  and  $1719 \pm 51$   $\text{L m}^{-2} \text{h}^{-1} \text{bar}^{-1}$ , respectively (Figure 5e). These data indicated that the introduction of THPC significantly improved the permeate flux of membrane. Simultaneously, the oil rejections of TCNF membranes for petroleum ether, chloroform, pump oil and dimethicone nano-emulsions were  $99.45 \pm 0.41\%$ ,  $99.19 \pm 0.16\%$ ,  $99.65 \pm 0.31\%$  and  $99.69 \pm 0.28\%$ , respectively, while the oil rejections of THPC@TCNF membranes for petroleum ether, chloroform, pump oil and dimethicone nano-emulsions were  $99.51 \pm 0.46\%$ ,  $99.23 \pm 0.23\%$ ,  $99.69 \pm 0.27\%$  and  $99.74 \pm 0.24\%$ , respectively (Figure 5f).

Despite that the introduction of THPC enlarged the pore size and enhanced the water permeate flux of the membrane, the oil rejections of THPC@TCNF membranes changed slightly and were maintained at high values.

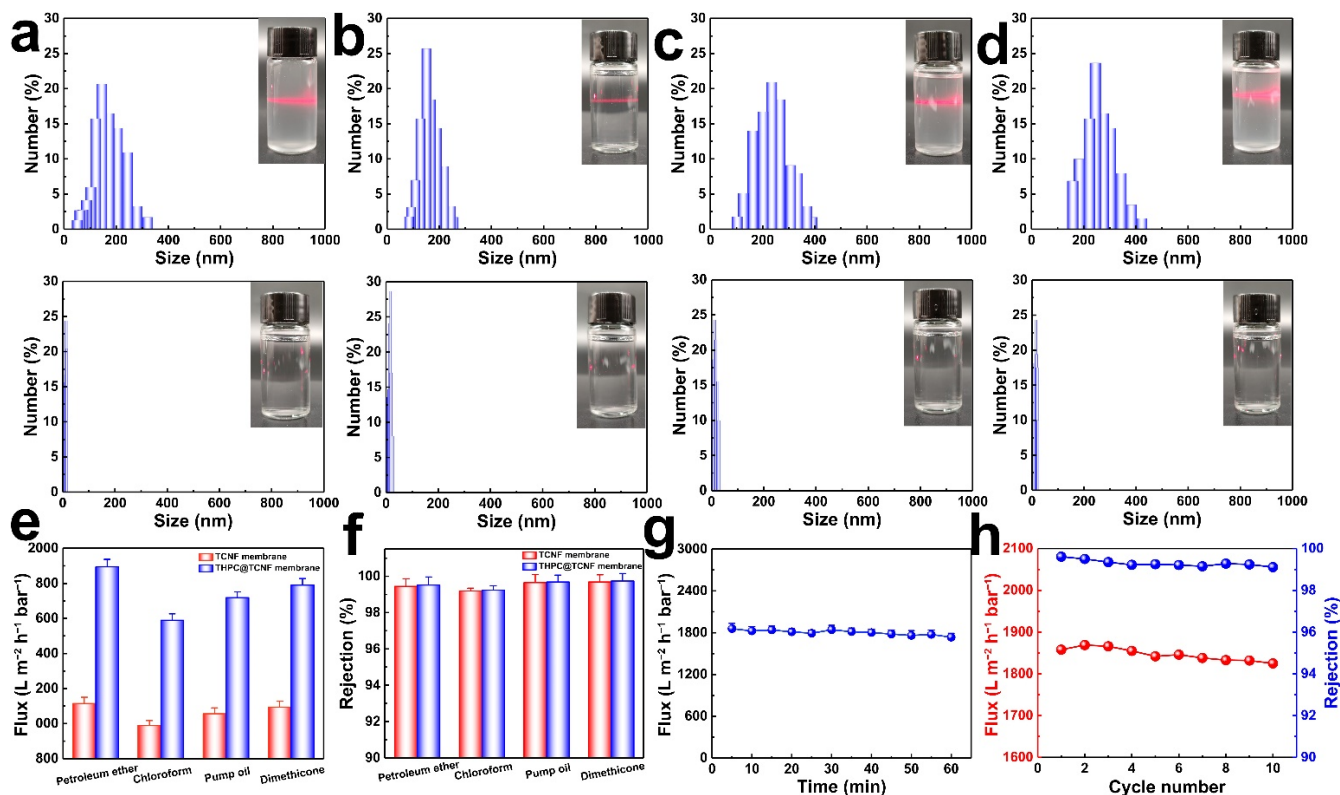


**Figure 5.** (a–d) Size distribution and photographs of oil/water nano-emulsions (petroleum ether, chloroform, pump oil and dimethicone) before (top) and after filtration (bottom). (e) Water permeate flux and (f) oil rejection of TCNF membrane and THPC@TCNF membrane. (g) The relationship between water permeate flux of THPC@TCNF membrane and separation time. (h) Cycle performance of THPC@TCNF membrane for the separation of petroleum ether/water nano-emulsion.

To investigate the durability of THPC@TCNF membrane, the separation of petroleum ether/water nano-emulsion for 60 min is displayed in Figure 5g. During the continuous separation of petroleum ether/water nano-emulsion, the water permeate flux of THPC@TCNF membrane was stable, which remained at  $1735 \pm 58 \text{ L m}^{-2} \text{ h}^{-1} \text{ bar}^{-1}$  after 60 min separation. Until 180 min, the flux was still higher than half of the initial flux and remained at  $1121 \pm 35 \text{ L m}^{-2} \text{ h}^{-1} \text{ bar}^{-1}$  (Figure S9a). In addition, as shown in Figure 5h, the cycle performance of THPC@TCNF membrane was also measured. Both water permeate flux and oil rejection of THPC@TCNF membrane hardly decreased after 10 cycles. Even after 20 cycles, the water flux slightly decreased to  $1523 \text{ L m}^{-2} \text{ h}^{-1} \text{ bar}^{-1}$ , while the oil rejection was still as high as 99.02% (Figure S9b), demonstrating excellent durability of THPC@TCNF membrane.

### 3.4. Antibacterial Activity and Mechanical Stability

The presence of bacteria in oily wastewater could decrease the separation efficiency of membranes during long-term use [49], so antibacterial properties of membranes are critical for the practical application of membranes. As shown in Figure 6a, a slight increase in the colony forming units on the TCNF membrane could be observed in comparison with the control group, because cellulose is a polysaccharide. Impressively, no colony of *B. subtilis* was observed on THPC@TCNF membrane because all *B. subtilis* were effectively killed after contacting with THPC@TCNF membrane for 1 h. Compared to control and TCNF

membrane, the antibacterial efficiency of THPC@TCNF membrane calculated according to the colony forming units before and after contact almost 100% (Figure 6b). After contacting with membranes for 1 h, the morphology of *B. subtilis* cultured on TCNF membrane was *B. subtilis*, whereas the surface of *B. subtilis* cultured on THPC@TCNF membrane became loose and fractured, as shown in Figure 6c and Figure S10, because quaternary phosphonium salts are capable of destroying a wide range of microorganisms by destabilizing bacterial cell walls [40]. The antibacterial property of HPC@TCNF membrane would be beneficial in preventing the corrosion of bacteria.

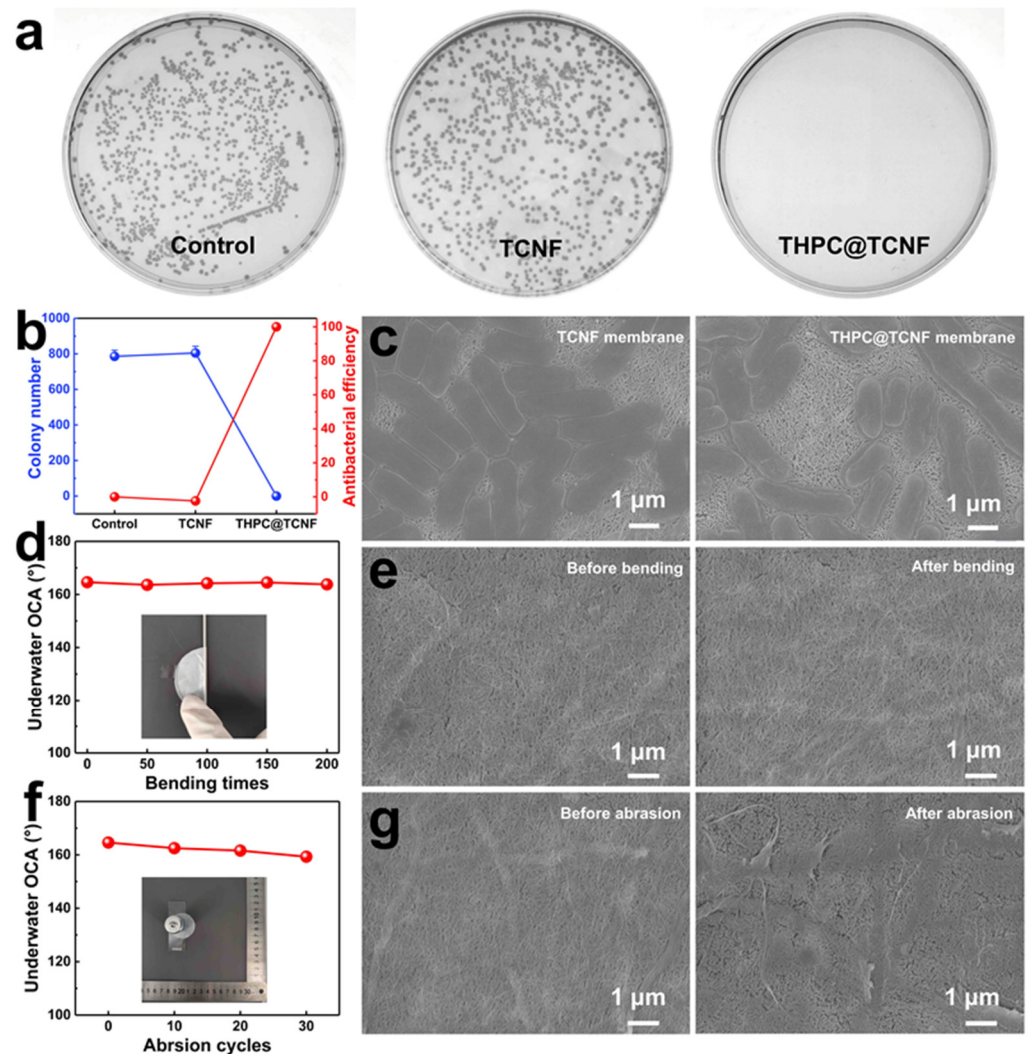


**Figure 6.** (a) Colony photographs after immersion test of control group, TCNF membrane and THPC@TCNF membrane against *B. subtilis* bacteria, respectively. (b) Corresponding statistics of the colony forming units and antibacterial efficiency. (c) SEM images of *B. subtilis* after contacting with TCNF membrane and THPC@TCNF membrane for 1 h. (d) Underwater OCA and (e) SEM image of THPC@TCNF membrane before and after bending test. (f) Underwater OCA and (g) SEM image of THPC@TCNF membrane before and after abrasion test.

Furthermore, both bending test and abrasion test were employed for evaluation of the mechanical stability of the THPC@TCNF membranes. As presented in Figure 6d, the pump oil contact angle still maintained at 163° after 200 bending cycles. The surface morphology of THPC@TCNF membrane hardly changed before and after the bending test (Figure 6e). Additionally, an abrasion test of THPC@TCNF membrane was also carried out by rubbing THPC@TCNF membrane on a 2000 mesh sandpaper (Figure 6f). The THPC@TCNF membrane was adhered to a glass slide with a weight of 100 g and the

membrane was subsequently dragged on the sandpaper for 10 cm in the horizontal and vertical directions, which constitutes a wear cycle. After 30 cycles, some fine moving traces appeared on the surface of the THPC@TCNF membrane, the complete structure of the membrane was not destroyed (Figure 6g). Simultaneously, the underwater OCA remained at an angle of  $159^\circ$  (Figure 6f), showing underwater superoleophobicity of the membrane. These results revealed that the THPC@TCNF membranes have good bending and wear resistance properties. Mechanical stability is a necessary condition to ensure long-term high-efficiency oil/water separation, which was beneficial to the practical application of THPC@TCNF membranes in the field of oil/water separation.

#### 4. Conclusions

We successfully fabricated THPC@TCNF membranes through grafting tetrahedral-structured THPC onto the surface of TCNFs *via* esterification reaction. THPC effectively increased the surface average pore size and interlayer spacing of TCNF membranes, resulting in the enhancement of water permeate flux of the membrane. On the other hand, the positively charged phosphonium groups endowed the TCNF membrane with good antibacterial properties, which could prevent the membrane from the corrosion of bacteria. These THPC@TCNF membranes exhibited good superhydrophilicity, underwater superoleophobicity and nano-porous structure, which enabled them to separate various oil/water nano-emulsions. Moreover, THPC@TCNF membranes possessed excellent durability, mechanical stability and cycle performance. This work provided a simple strategy for fabricating high water permeate flux and antibacterial membranes, which has great potential in oily wastewater treatment.

**Supplementary Materials:** The following supporting information can be downloaded at: <https://www.mdpi.com/article/10.3390/coatings12101598/s1>, Figure S1: Photographs of TCNF membrane (a) and THPC@TCNF membrane (b); Figure S2: Characterization of the morphology, length and height distribution of TCNFs; Figure S3: Photograph of TCNFs suspension; Figure S4: TEM images of TCNFs before (a) and after modified with THPC (b); Figure S5: High-resolution  $P_{2p}$  spectra of TCNF membrane and THPC@TCNF membrane; Figure S6: EDS mapping of chlorine element on THPC@TCNF membrane; Figure S7: Various oil droplets on TCNF membrane underwater; Figure S8: Water flux of THPC@TCNF membranes with different THPC content; Figure S9: (a) Water flux of THPC@TCNF membrane during continuous separation and (b) cycling performance of THPC@TCNF membrane for petroleum ether/water nano-emulsion; Figure S10: SEM images of *B. subtilis* after contacting with TCNF membrane (a) and THPC@TCNF membrane (b) for 1 h.

**Author Contributions:** Conceptualization, K.P., C.C. and N.P.; methodology, K.P.; software, K.P.; validation, K.P.; formal analysis, K.P. and C.W.; investigation, K.P.; resources, C.W.; data curation, K.P.; writing—original draft preparation, K.P.; writing—review and editing, C.C.; visualization, K.P.; supervision, C.C. and N.P.; project administration, C.C. and N.P.; funding acquisition, C.C. All authors have read and agreed to the published version of the manuscript.

**Funding:** This work was financially supported by the National Key Research and Development Program of China (2018YFE0123700), the National Natural Science Foundation of China (52073217, 51873164) and Key Research and Development Program of Hubei Province (2020BCA079).

**Institutional Review Board Statement:** Not applicable.

**Informed Consent Statement:** Not applicable.

**Data Availability Statement:** Not applicable.

**Conflicts of Interest:** The authors declare no competing financial interest.

#### References

1. Gupta, R.K.; Dunderdale, G.J.; England, M.W.; Hozumi, A. Oil/water separation techniques: A review of recent progresses and future directions. *J. Mater. Chem. A* **2017**, *5*, 16025–16058. [[CrossRef](#)]
2. Liu, Y.; Wang, X.; Feng, S. Nonflammable and Magnetic Sponge Decorated with Polydimethylsiloxane Brush for Multitasking and Highly Efficient Oil–Water Separation. *Adv. Funct. Mater.* **2019**, *29*, 1902488. [[CrossRef](#)]

3. Peng, Y.; Guo, Z. Recent advances in biomimetic thin membranes applied in emulsified oil/water separation. *J. Mater. Chem. A* **2016**, *4*, 15749–15770. [[CrossRef](#)]
4. Kamcev, J.; Taylor, M.K.; Shin, D.M.; Jarenwattananon, N.N.; Colwell, K.A.; Long, J.R. Functionalized Porous Aromatic Frameworks as High-Performance Adsorbents for the Rapid Removal of Boric Acid from Water. *Adv. Mater.* **2019**, *31*, e1808027. [[CrossRef](#)] [[PubMed](#)]
5. Yu, X.; Zhu, Y.; Cheng, C.; Zhang, T.; Wang, X.; Hsiao, B.S. Novel thin-film nanofibrous composite membranes containing directional toxin transport nanochannels for efficient and safe hemodialysis application. *J. Membr. Sci.* **2019**, *582*, 151–163. [[CrossRef](#)]
6. Zheng, W.; Huang, J.; Li, S.; Ge, M.; Teng, L.; Chen, Z.; Lai, Y. Advanced Materials with Special Wettability toward Intelligent Oily Wastewater Remediation. *ACS Appl. Mater. Interfaces* **2021**, *13*, 67–87. [[CrossRef](#)] [[PubMed](#)]
7. Deng, Y.Y.; Peng, C.S.; Dai, M.; Lin, D.C.; Ali, I.; Alhewairini, S.S.; Zheng, X.L.; Chen, G.Q.; Li, J.Y.; Naz, I. Recent development of super-wettable materials and their applications in oil-water separation. *J. Clean Prod.* **2020**, *266*, 121624. [[CrossRef](#)]
8. Zhan, H.; Zuo, T.; Tao, R.J.; Chang, C.Y. Robust Tunicate Cellulose Nanocrystal/Palygorskite Nanorod Membranes for Multifunctional Oil/Water Emulsion Separation. *ACS Sustain. Chem. Eng.* **2018**, *6*, 10833–10840. [[CrossRef](#)]
9. Peng, K.; Huang, Y.; Peng, N.; Chang, C.Y. Antibacterial nanocellulose membranes coated with silver nanoparticles for oil/water emulsions separation. *Carbohydr. Polym.* **2022**, *278*, 118929. [[CrossRef](#)] [[PubMed](#)]
10. Cai, Y.; Chen, D.; Li, N.; Xu, Q.; Li, H.; He, J.; Lu, J. A Self-Cleaning Heterostructured Membrane for Efficient Oil-in-Water Emulsion Separation with Stable Flux. *Adv. Mater.* **2020**, *32*, e2001265. [[CrossRef](#)]
11. Damodar, R.A.; You, S.J.; Chou, H.H. Study the self cleaning, antibacterial and photocatalytic properties of TiO<sub>2</sub> entrapped PVDF membranes. *J. Hazard. Mater.* **2009**, *172*, 1321–1328. [[CrossRef](#)] [[PubMed](#)]
12. Zhu, M.; Wang, Y.; Zhu, S.; Xu, L.; Jia, C.; Dai, J.; Song, J.; Yao, Y.; Wang, Y.; Li, Y.; et al. Anisotropic, Transparent Films with Aligned Cellulose Nanofibers. *Adv. Mater.* **2017**, *29*, 1606284. [[CrossRef](#)] [[PubMed](#)]
13. Benito, J.M.; Sánchez, M.J.; Pena, P.; Rodríguez, M.A. Development of a new high porosity ceramic membrane for the treatment of bilge water. *Desalination* **2007**, *214*, 91–101. [[CrossRef](#)]
14. Shi, Z.; Zhang, W.; Zhang, F.; Liu, X.; Wang, D.; Jin, J.; Jiang, L. Ultrafast Separation of Emulsified Oil/Water Mixtures by Ultrathin Free-Standing Single-Walled Carbon Nanotube Network Films. *Adv. Mater.* **2013**, *25*, 2422–2427. [[CrossRef](#)] [[PubMed](#)]
15. Chen, C.; Hu, L. Nanocellulose toward Advanced Energy Storage Devices: Structure and Electrochemistry. *Acc. Chem. Res.* **2018**, *51*, 3154–3165. [[CrossRef](#)] [[PubMed](#)]
16. Heise, K.; Kontturi, E.; Allahverdiyeva, Y.; Tammelin, T.; Linder, M.B.; Nonappa; Ikkala, O. Nanocellulose: Recent Fundamental Advances and Emerging Biological and Biomimicking Applications. *Adv. Mater.* **2021**, *33*, e2004349. [[CrossRef](#)] [[PubMed](#)]
17. Isogai, A. Emerging Nanocellulose Technologies: Recent Developments. *Adv. Mater.* **2021**, *33*, e2000630. [[CrossRef](#)]
18. De France, K.; Zeng, Z.; Wu, T.; Nystrom, G. Functional Materials from Nanocellulose: Utilizing Structure-Property Relationships in Bottom-Up Fabrication. *Adv. Mater.* **2021**, *33*, e2000657. [[CrossRef](#)]
19. Cheng, Q.Y.; Ye, D.D.; Chang, C.Y.; Zhang, L.N. Facile fabrication of superhydrophilic membranes consisted of fibrous tunicate cellulose nanocrystals for highly efficient oil/water separation. *J. Membr. Sci.* **2017**, *525*, 1–8. [[CrossRef](#)]
20. Norfarhana, A.S.; Ilyas, R.A.; Ngadi, N. A review of nanocellulose adsorptive membrane as multifunctional wastewater treatment. *Carbohydr. Polym.* **2022**, *291*, 119563. [[CrossRef](#)]
21. Wang, Z.H.; Chen, Z.; Zheng, Z.D.; Liu, H.Z.; Zhu, L.P.; Yang, M.C.; Chen, Y. Nanocellulose-based membranes for highly efficient molecular separation. *Chem. Eng. J.* **2023**, *451*, 138711. [[CrossRef](#)]
22. Das, R.; Lindstrom, T.; Sharma, P.R.; Chi, K.; Hsiao, B.S. Nanocellulose for sustainable water purification. *Chem. Rev.* **2022**, *122*, 8936–9031. [[CrossRef](#)] [[PubMed](#)]
23. Wang, Q.Q.; Liu, S.M.; Liu, J.; Sun, J.Z.; Zhang, Z.; Zhu, Q.Q. Sustainable cellulose nanomaterials for environmental remediation—Achieving clean air, water, and energy: A review. *Carbohydr. Polym.* **2022**, *285*, 119251. [[CrossRef](#)]
24. Yan, J.; Bai, T.; Yue, Y.Y.; Cheng, W.L.; Bai, L.; Wang, D.; Lu, J.Q.; Cao, M.L.; Shi, S.Q.; Huan, S.Q.; et al. Nanostructured superior oil-adsorbent nanofiber composites using one-step electrospinning of polyvinylidene fluoride/nanocellulose. *Compos. Sci. Technol.* **2022**, *224*, 109490. [[CrossRef](#)]
25. Wang, Z.H.; Xia, D.W.; Wang, B.T.; Liu, H.Z.; Zhu, L.P. Highly permeable polyamide nanofiltration membrane incorporated with phosphorylated nanocellulose for enhanced desalination. *J. Membr. Sci.* **2022**, *647*, 120339. [[CrossRef](#)]
26. Wang, Q.X.; Wang, D.; Cheng, W.L.; Huang, J.Q.; Cao, M.L.; Niu, Z.X.; Zhao, Y.Y.; Yue, Y.Y.; Han, G.P. Spider-web-inspired membrane reinforced with thiol-functionalized cellulose nanocrystals for oil/water separation. *Carbohydr. Polym.* **2022**, *282*, 119049. [[CrossRef](#)] [[PubMed](#)]
27. Xia, D.W.; Zhang, M.X.; Tong, C.C.; Wang, Z.H.; Liu, H.Z.; Zhu, L.P. In-situ incorporating zwitterionic nanocellulose into polyamide nanofiltration membrane towards excellent perm-selectivity and antifouling performances. *Desalination* **2022**, *521*, 115397. [[CrossRef](#)]
28. Lehtonen, J.; Chen, X.; Beaumont, M.; Hassinen, J.; Orelma, H.; Dumee, L.F.; Tardy, B.L.; Rojas, O.J. Impact of incubation conditions and post-treatment on the properties of bacterial cellulose membranes for pressure-driven filtration. *Carbohydr. Polym.* **2021**, *251*, 117073. [[CrossRef](#)]
29. Pak, S.; Ahn, J.; Kim, H. High performance and sustainable CNF membrane via facile in-situ envelopment of hydrochar for water treatment. *Carbohydr. Polym.* **2022**, *296*, 119948. [[CrossRef](#)]

30. Hu, Y.; Yue, M.; Yuan, F.S.; Yang, L.Y.; Chen, C.T.; Sun, D.P. Bio-inspired fabrication of highly permeable and anti-fouling ultrafiltration membranes based on bacterial cellulose for efficient removal of soluble dyes and insoluble oils. *J. Membr. Sci.* **2021**, *621*, 118982. [[CrossRef](#)]
31. Kwon, H.J.; Lee, M.; Hong, S.K.; Park, C.; Cho, S.J.; Lim, G. Comprehensive Electrokinetic-Assisted Separation of Oil Emulsion with Ultrahigh Flux. *ACS Nano* **2021**, *15*, 15815–15823. [[CrossRef](#)]
32. Hu, L.; Gao, S.; Ding, X.; Wang, D.; Jiang, J.; Jin, J.; Jiang, L. Photothermal-Responsive Single-Walled Carbon Nanotube-Based Ultrathin Membranes for On/Off Switchable Separation of Oil-in-Water Nanoemulsions. *ACS Nano* **2015**, *9*, 4835–4842. [[CrossRef](#)]
33. Lamm, M.E.; Li, K.; Qian, J.; Wang, L.; Lavoine, N.; Newman, R.; Gardner, D.J.; Li, T.; Hu, L.; Ragauskas, A.J.; et al. Recent Advances in Functional Materials through Cellulose Nanofiber Templating. *Adv. Mater.* **2021**, *33*, 2005538. [[CrossRef](#)]
34. Li, T.; Chen, C.; Brozena, A.H.; Zhu, J.Y.; Xu, L.; Driemeier, C.; Dai, J.; Rojas, O.J.; Isogai, A.; Wagberg, L.; et al. Developing fibrillated cellulose as a sustainable technological material. *Nature* **2021**, *590*, 47–56. [[CrossRef](#)] [[PubMed](#)]
35. Ke, W.T.; Chiu, H.L.; Liao, Y.C. Multifunctionalized Cellulose Nanofiber for Water-Repellent and Wash-Sustainable Coatings on Fabrics. *Langmuir* **2020**, *36*, 8144–8151. [[CrossRef](#)] [[PubMed](#)]
36. Wahid, F.; Zhao, X.J.; Duan, Y.X.; Zhao, X.Q.; Jia, S.R.; Zhong, C. Designing of bacterial cellulose-based superhydrophobic/underwater superoleophobic membrane for oil/water separation. *Carbohydr. Polym.* **2021**, *257*, 117611. [[CrossRef](#)]
37. Orsolini, P.; Marchesi D'Alvise, T.; Boi, C.; Geiger, T.; Caseri, W.R.; Zimmermann, T. Nanofibrillated Cellulose Templated Membranes with High Permeance. *ACS Appl. Mater. Interfaces* **2016**, *8*, 33943–33954. [[CrossRef](#)]
38. Tang, N.; Li, Y.; Ge, J.; Si, Y.; Yu, J.; Yin, X.; Ding, B. Ultrathin Cellulose Voronoi-Nanonet Membranes Enable High-Flux and Energy-Saving Water Purification. *ACS Appl. Mater. Interfaces* **2020**, *12*, 31852–31862. [[CrossRef](#)] [[PubMed](#)]
39. Olkiewicz, M.; Caporgno, M.P.; Font, J.; Legrand, J.; Lepine, O.; Plechkova, N.V.; Pruvost, J.; Seddon, K.R.; Bengoa, C. A novel recovery process for lipids from microalgae for biodiesel production using a hydrated phosphonium ionic liquid. *Green Chem.* **2015**, *17*, 2813–2824. [[CrossRef](#)]
40. Peng, H.; Zhang, W.H.; Hung, W.S.; Wang, N.; Sun, J.; Lee, K.R.; An, Q.F.; Liu, C.M.; Zhao, Q. Phosphonium Modification Leads to Ultrapermeable Antibacterial Polyamide Composite Membranes with Unreduced Thickness. *Adv. Mater.* **2020**, *32*, e2001383. [[CrossRef](#)] [[PubMed](#)]
41. Palermo, E.F.; Lienkamp, K.; Gillies, E.R.; Ragona, P.J. Antibacterial Activity of Polymers: Discussions on the Nature of Amphiphilic Balance. *Angew. Chem. Int. Ed.* **2019**, *58*, 3690–3693. [[CrossRef](#)] [[PubMed](#)]
42. Huang, Y.N.; Zhan, H.; Li, D.; Tian, H.F.; Chang, C.Y. Tunicate cellulose nanocrystals modified commercial filter paper for efficient oil/water separation. *J. Membr. Sci.* **2019**, *591*, 117362. [[CrossRef](#)]
43. Cheng, Q.Y.; Ye, D.D.; Yang, W.T.; Zhang, S.H.; Chen, H.Z.; Chang, C.Y.; Zhang, L.N. Construction of Transparent Cellulose-Based Nanocomposite Papers and Potential Application in Flexible Solar Cells. *ACS Sustain. Chem. Eng.* **2018**, *6*, 8040–8047. [[CrossRef](#)]
44. Zhang, Y.Y.; Cheng, Q.Y.; Chang, C.Y.; Zhang, L.N. Phase transition identification of cellulose nanocrystal suspensions derived from various raw materials. *J. Appl. Polym. Sci.* **2018**, *135*, 45702. [[CrossRef](#)]
45. Isogai, A.; Saito, T.; Fukuzumi, H. TEMPO-oxidized cellulose nanofibers. *Nanoscale* **2011**, *3*, 71–85. [[CrossRef](#)] [[PubMed](#)]
46. Kang, X.; Sun, P.; Kuga, S.; Wang, C.; Zhao, Y.; Wu, M.; Huang, Y. Thin Cellulose Nanofiber from Corn Cob Cellulose and Its Performance in Transparent Nanopaper. *ACS Sustain. Chem. Eng.* **2017**, *5*, 2529–2534. [[CrossRef](#)]
47. Li, D.; Yuan, J.; Cheng, Q.Y.; Wei, P.; Cheng, G.J.; Chang, C.Y. Additive printing of recyclable anti-counterfeiting patterns with sol-gel cellulose nanocrystal inks. *Nanoscale* **2021**, *13*, 11808–11816. [[CrossRef](#)] [[PubMed](#)]
48. Zhang, W.F.; Liu, N.; Cao, Y.Z.; Lin, X.; Liu, Y.N.; Feng, L. Superwetting Porous Materials for Wastewater Treatment: From Immiscible Oil/Water Mixture to Emulsion Separation. *Adv. Mater. Interfaces* **2017**, *4*, 1600029. [[CrossRef](#)]
49. Bethke, K.; Palantoken, S.; Andrei, V.; Ross, M.; Raghuvanshi, V.S.; Kettemann, F.; Greis, K.; Ingber, T.T.K.; Stuckrath, J.B.; Valiyaveetil, S.; et al. Functionalized Cellulose for Water Purification, Antimicrobial Applications, and Sensors. *Adv. Funct. Mater.* **2018**, *28*, 1800409. [[CrossRef](#)]